

DEEP LEARNING BASED HYBRID PRECODING IN DUAL-BAND COMMUNICATION SYSTEMS

Rafail Ismayilov*, Renato L. G. Cavalcante*[†] and Sławomir Stańczak*[†]

*Fraunhofer Heinrich Hertz Institute, Berlin, Germany

[†]Technical University of Berlin, Berlin, Germany

ABSTRACT

We propose a deep learning-based method that uses spatial and temporal information extracted from the sub-6GHz band to predict/track beams in the millimeter-wave (mmWave) band. In more detail, we consider a dual-band communication system operating in both the sub-6GHz and mmWave bands. The objective is to maximize the achievable mutual information in the mmWave band with a hybrid analog/digital architecture where analog precoders (RF precoders) are taken from a finite codebook. Finding a RF precoder using conventional search methods incurs large signalling overhead, and the signalling scales with the number of RF chains and the resolution of the phase shifters. To overcome the issue of large signalling overhead in the mmWave band, the proposed method exploits the spatiotemporal correlation between sub-6GHz and mmWave bands, and it predicts/tracks the RF precoders in the mmWave band from sub-6GHz channel measurements. The proposed method provides a smaller candidate set so that performing a search over that set significantly reduces the signalling overhead compared with conventional search heuristics. Simulations show that the proposed method can provide reasonable achievable rates while significantly reducing the signalling overhead.

Index Terms— Hybrid beamforming, dual-band communication, millimeter wave, deep learning

1. INTRODUCTION

Integrated networks that enable simultaneous usage of sub-6GHz and mmWave bands have been considered as built-in technology in 5G [1]. Unlike the conventional sub-6GHz band, the signal processing in mmWave band is typically accomplished in both the analog and digital domains [2]. One of the main challenges in these hybrid systems is that conventional channel estimation methods typically used in the sub-6GHz band cannot be straightforwardly used in mmWave systems. The reason is that in mmWave systems with hybrid architectures the channel measured in the digital baseband is intertwined with the choice of analog precoders (RF precoders), and thus the entries of the channel matrix cannot be directly accessed. As a result, new methods are required to find both the analog and digital parameters in mmWave systems with hybrid architectures. In particular, the channel experienced by the receiver is affected by the choice of RF precoder, which is usually selected from a finite codebook, and it includes the beams in a particular angular direction. To find the best mmWave beam (e.g., the angular direction of the strongest signal) the transmitter and receiver need to perform an exhaustive search over all possible beam patterns [3]. An exhaustive search, in turn, creates a signalling overhead that scales with the receiver mobility and the codebook resolution.

To improve existing search heuristics by decreasing the search space, we propose to exploit the spatial correlation between sub-6GHz and mmWave bands, which has been observed by experimental measurements [4–6]. Related techniques have been considered,

for example, in [4], where the authors use sub-6GHz spatial information to discover the mmWave line-of-sight (LoS) direction. With the same goal, the authors in [7] have introduced a strategy to extract the spatial information from sub-6GHz, and they use it in mmWave compressed beam-selection, assuming an analog architecture at the mmWave band. Closer to the objective of this work, the study of deep learning methods for mmWave beamforming, based on sub-6GHz channels information, is considered in [8]. Although the proposed methods in [4, 7, 8] are reducing the beam training overhead, none of the proposed methods consider a hybrid beamforming (HBF) architecture in the mmWave band. Moreover, the above-cited works are mainly limited to predict current mmWave beams given current sub-6GHz channel measurements, but beam prediction from the spatially and temporally correlated sub-6GHz channel measurements have not been studied.

In contrast to previous studies, we consider important practical components in wireless communication systems, including non-line-of-sight (NLOS) propagation and antenna polarization. Moreover, the proposed method tracks future beams given past sub-6GHz channel measurements, which is a new aspect to the best of our knowledge. The idea of predicting future beams from past sub-6GHz channel measurements is motivated by the spatial consistency of two close locations [9]. For example, with user equipment (UE) mobility, the measured channels in two closely spaced UE locations are often observed to have similar parameters such as the angle-of-arrival (AoA). Hence, we use a neural network to exploit the sequence of sub-6GHz channel measurements, which are correlated in both spatial and time domain, to predict the mmWave beam in the next time step(s). In addition, we improve the prediction performance by fusing side-information such as the UE location. In particular, the proposed network design provides us with an opportunity to reduce the beam search space significantly if standard beam alignment strategies are employed. We evaluate the performance of the proposed method with numerical simulations, and we compare it with the conventional search heuristics.

2. SYSTEM MODEL AND PROBLEM STATEMENT

2.1. System Model

In the following, we consider a dual-band wireless multiple-input multiple-output (MIMO)-orthogonal frequency division multiplexing (OFDM) communication system operating in both sub-6GHz and mmWave bands, and consisting of single base station (BS) and single UE. The BS is assumed to employ a uniform planar array (UPA) with $N_{\text{tx}}^{\text{sub-6}}$ and N_{tx} antenna elements with cross-polarization in the sub-6GHz and mmWave bands, respectively. The UE is assumed to employ a single antenna in sub-6GHz and a UPA with N_{rx} antenna elements in mmWave band. The total number of OFDM subcarriers in the sub-6GHz and mmWave bands are denoted by K and \bar{K} , respectively. In this work, we exploit the uplink channel measurements in the sub-6GHz band to assist the beamforming in the downlink mmWave band. With cross-polarization, the uplink sub-6GHz channel at subcarrier $k \in \{1, \dots, K\}$ and the down-

link mmWave channel at subcarrier $\bar{k} \in \{1, \dots, \bar{K}\}$ are denoted by $\mathbf{h}[\bar{k}] \in \mathbb{C}^{2N_{\text{tx}}^{\text{sub-6}}}$ and $\mathbf{H}[\bar{k}] \in \mathbb{C}^{2N_{\text{tx}} \times 2N_{\text{tx}}}$, respectively. We assume that the UE can perform optimal decoding from a received signal in the mmWave band with fully digital hardware, and we focus on the hybrid precoding design at the BS. An illustration of the hybrid precoding architecture in the mmWave band with N_s data streams, N_{RF} RF chains, and N_{tx} transmit antennas with cross-polarization is given in Fig. 1. Let $\mathbf{F}_{\text{RF}} \in \mathbb{C}^{2N_{\text{tx}} \times N_{\text{RF}}}$ be an RF precoding matrix, and $\mathbf{F}[\bar{k}] \in \mathbb{C}^{N_{\text{RF}} \times N_s}$ be a digital baseband precoding matrix at the \bar{k} th OFDM subcarrier in the mmWave band. The RF precoder is decomposed into a $+45^\circ$ polarized precoder $\widehat{\mathbf{F}}_{\text{RF}} \in \mathbb{C}^{N_{\text{tx}} \times N_{\text{RF}}}$ and a -45° polarized precoder $\widetilde{\mathbf{F}}_{\text{RF}} \in \mathbb{C}^{N_{\text{tx}} \times N_{\text{RF}}}$, and we define $\mathbf{F}_{\text{RF}} := \left[\widehat{\mathbf{F}}_{\text{RF}}^T \widetilde{\mathbf{F}}_{\text{RF}}^T \right]^T$. The received signal at subcarrier \bar{k} for a transmitted symbol $\mathbf{s}[\bar{k}] \in \mathbb{C}^{N_s}$ is given by

$$\mathbf{y}[\bar{k}] = \mathbf{H}[\bar{k}] \mathbf{F}_{\text{RF}} \mathbf{F}[\bar{k}] \mathbf{s}[\bar{k}] + \mathbf{n}[\bar{k}], \quad (1)$$

where $\mathbf{n}[\bar{k}] \in \mathbb{C}^{2N_{\text{tx}}}$ denotes the additive white Gaussian noise. The cross-polarized mmWave channel at subcarrier \bar{k} is represented in block form as

$$\mathbf{H}[\bar{k}] = \begin{bmatrix} \mathbf{H}[\bar{k}]_{+45^\circ} & \mathbf{H}[\bar{k}]_{\pm 45^\circ} \\ \mathbf{H}[\bar{k}]_{\mp 45^\circ} & \mathbf{H}[\bar{k}]_{-45^\circ} \end{bmatrix}, \quad (2)$$

where the diagonal blocks $\mathbf{H}[\bar{k}]_{+45^\circ}$ and $\mathbf{H}[\bar{k}]_{-45^\circ}$ represent the co-polarized, and the off-diagonal blocks $\mathbf{H}[\bar{k}]_{\pm 45^\circ}$ and $\mathbf{H}[\bar{k}]_{\mp 45^\circ}$ represent the cross-polarized components. In this work, we consider a hybrid precoding design with fixed subarray architecture, which means that each RF chain is connected to one of the non-overlapping subsets of antenna elements (see Fig. 1). For simplicity, we assume that all RF chains have the same subset size. With this architecture, the analog precoding matrix with $+45^\circ$ polarization takes the form of a block diagonal matrix as follows:

$$\widehat{\mathbf{F}}_{\text{RF}} = \text{blkdiag}(\widehat{\mathbf{f}}_1, \dots, \widehat{\mathbf{f}}_{N_{\text{RF}}}) = \begin{bmatrix} \widehat{\mathbf{f}}_1 & \dots & \mathbf{0} \\ \vdots & \ddots & \vdots \\ \mathbf{0} & \dots & \widehat{\mathbf{f}}_{N_{\text{RF}}} \end{bmatrix},$$

where $(\forall r \in \{1, \dots, N_{\text{RF}}\}) \widehat{\mathbf{f}}_r$ are design parameters. The RF precoding matrix with -45° polarization is defined in a similar way; i.e., $\widetilde{\mathbf{F}}_{\text{RF}} = \text{blkdiag}(\widetilde{\mathbf{f}}_1, \dots, \widetilde{\mathbf{f}}_{N_{\text{RF}}})$. In the above, $(\forall r \in \{1, \dots, N_{\text{RF}}\}) \widehat{\mathbf{f}}_r, \widetilde{\mathbf{f}}_r \in \mathbb{C}^{N_{\text{tx}}/N_{\text{RF}}}$ is a beamforming vector associated with the r th RF chain, and we assume that each beamforming vector is selected from a predefined finite codebook \mathcal{C} , i.e., $(\forall r \in \{1, \dots, N_{\text{RF}}\}) \widehat{\mathbf{f}}_r, \widetilde{\mathbf{f}}_r \in \mathcal{C}$ [10].

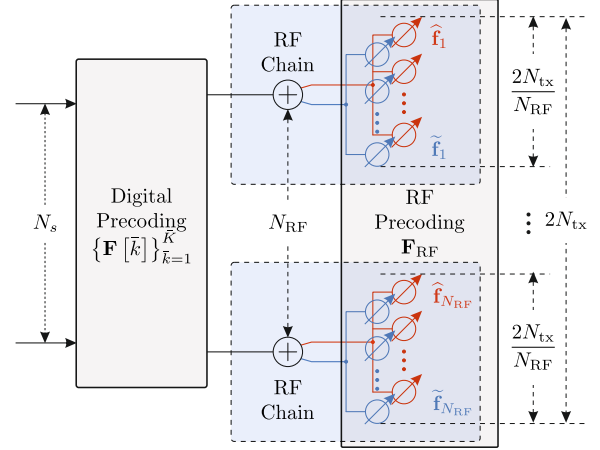


Fig. 1. Hybrid analog/digital precoding architecture in a mmWave band MIMO-OFDM system with cross-polarization.

2.2. Problem Statement

Assuming that the symbols are sampled from a Gaussian distribution, i.e., $\mathbf{s}[\bar{k}] \sim \mathcal{N}(\mathbf{0}, \mathbf{I})$ [11, 12], a general approach for hybrid precoding is to maximize the mutual information given in (3) at the bottom of this page, where ρ denotes the signal-to-noise ratio (SNR). Optimizing (3) directly is challenging due to (i) the non-convex constraint on \mathbf{F}_{RF} , and (ii) the coupling between the analog and digital matrices, which arises in the power constraint. Alternatively, it is shown in [13, 14] that the optimal digital precoder can be written as a function of the optimal RF precoders \mathbf{F}_{RF}^* , e.g., $(\forall \bar{k} \in \{1, \dots, \bar{K}\}) \mathbf{F}^*[\bar{k}] = f(\mathbf{F}_{\text{RF}}^*)$ where $f: \mathbb{C}^{2N_{\text{tx}} \times N_{\text{RF}}} \rightarrow \mathbb{C}^{N_{\text{RF}} \times N_s}$ is a known function given in [13, 14]. This enables us to focus on the optimization of the RF precoder \mathbf{F}_{RF}^* , since the digital precoder $(\forall \bar{k} \in \{1, \dots, \bar{K}\}) \mathbf{F}^*[\bar{k}]$ can be easily recovered from \mathbf{F}_{RF}^* with the function f . Using the relation between digital and analog precoders, i.e., $(\forall \bar{k} \in \{1, \dots, \bar{K}\}) \mathbf{F}^*[\bar{k}] = f(\mathbf{F}_{\text{RF}}^*)$, we can remove the digital precoders from (3). Effectively, this leads to the new problem in (4) where the mutual information-based hybrid precoding is determined only by the RF precoders.

Although the formulation in (4) simplifies the hybrid precoding problem, the optimization is still hard owing to the discrete constraints imposed on the analog precoder \mathbf{F}_{RF} . In principle, the problem in (4) could be solved via exhaustive search. Performing this search, however, requires either estimating the mmWave channel \mathbf{H} or an online exhaustive beam training, but both approaches have a large signalling overhead. In the following, we propose a deep learning-based method that predicts the RF precoders from sub-6GHz channel measurements.

$$\left\{ \mathbf{F}_{\text{RF}}^*, \{ \mathbf{F}^*[\bar{k}] \}_{\bar{k}=1}^{\bar{K}} \right\} \in \arg \max_{\mathbf{F}_{\text{RF}}, \{ \mathbf{F}[\bar{k}] \}_{\bar{k}=1}^{\bar{K}}} \sum_{\bar{k}=1}^{\bar{K}} \log_2 \left| \mathbf{I} + \rho \mathbf{H}[\bar{k}] \mathbf{F}_{\text{RF}} \mathbf{F}[\bar{k}] \mathbf{F}^H[\bar{k}] \mathbf{F}_{\text{RF}}^H \mathbf{H}^H[\bar{k}] \right|$$

such that $\mathbf{F}_{\text{RF}} \in \left\{ \left[\widehat{\mathbf{F}}_{\text{RF}}^T \widetilde{\mathbf{F}}_{\text{RF}}^T \right]^T \mid \widehat{\mathbf{F}}_{\text{RF}} = \text{blkdiag}(\widehat{\mathbf{f}}_1, \dots, \widehat{\mathbf{f}}_{N_{\text{RF}}}), \widetilde{\mathbf{F}}_{\text{RF}} = \text{blkdiag}(\widetilde{\mathbf{f}}_1, \dots, \widetilde{\mathbf{f}}_{N_{\text{RF}}}) \right\}$, and $(\forall r \in \{1, \dots, N_{\text{RF}}\}) \widehat{\mathbf{f}}_r, \widetilde{\mathbf{f}}_r \in \mathcal{C}$ } , (3)

$$\sum_{\bar{k}=1}^{\bar{K}} \left\| \mathbf{F}_{\text{RF}} \mathbf{F}[\bar{k}] \right\|^2 = \bar{K} N_s.$$

$$\mathbf{F}_{\text{RF}}^* \in \arg \max_{\mathbf{F}_{\text{RF}}} \sum_{\bar{k}=1}^{\bar{K}} \log_2 \left| \mathbf{I} + \rho \mathbf{H}[\bar{k}] \mathbf{F}_{\text{RF}} \left(\mathbf{F}_{\text{RF}}^H \mathbf{F}_{\text{RF}} \right)^{-1} \mathbf{F}_{\text{RF}}^H \mathbf{H}^H[\bar{k}] \right|$$

such that $\mathbf{F}_{\text{RF}} \in \left\{ \left[\widehat{\mathbf{F}}_{\text{RF}}^T \widetilde{\mathbf{F}}_{\text{RF}}^T \right]^T \mid \widehat{\mathbf{F}}_{\text{RF}} = \text{blkdiag}(\widehat{\mathbf{f}}_1, \dots, \widehat{\mathbf{f}}_{N_{\text{RF}}}), \widetilde{\mathbf{F}}_{\text{RF}} = \text{blkdiag}(\widetilde{\mathbf{f}}_1, \dots, \widetilde{\mathbf{f}}_{N_{\text{RF}}}) \right\}$. and $(\forall r \in \{1, \dots, N_{\text{RF}}\}) \widehat{\mathbf{f}}_r, \widetilde{\mathbf{f}}_r \in \mathcal{C}$ } . (4)

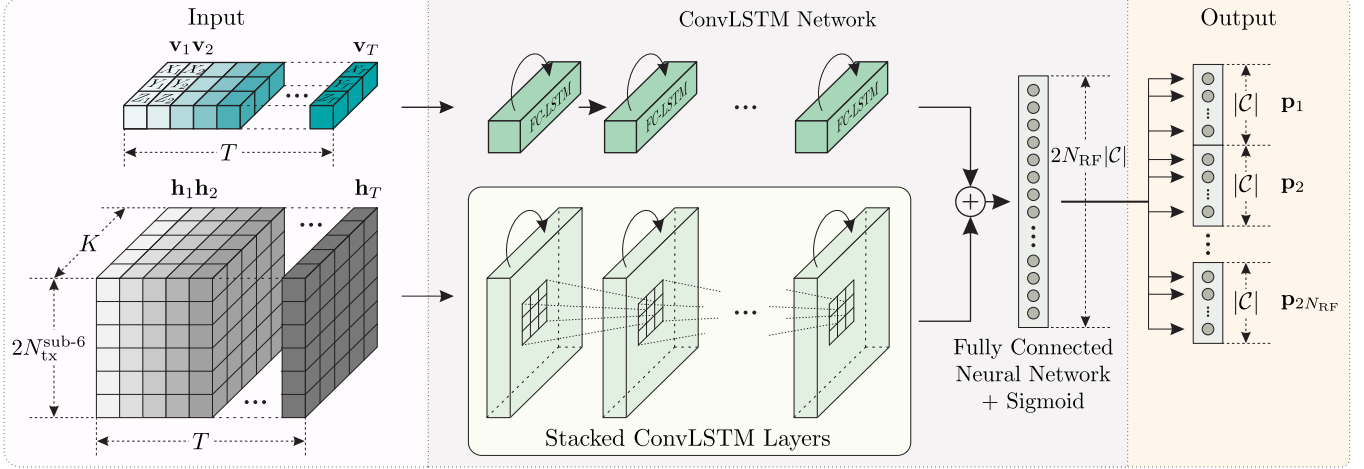


Fig. 2. The proposed neural network architecture for beam prediction/tracking. The network takes the spatiotemporal sub-6GHz channel measurements with T samples in sequence and predicts the mmWave beam indices in $T + 1$ time step.

3. DEEP LEARNING-BASED HYBRID PRECODING

To cope with the problem in (4), we assume that there exists an ideal mapping Ξ that maps the sequence of T sub-6GHz channel measurements $[\mathbf{h}_1, \dots, \mathbf{h}_T]$ in the uplink to some output $[\mathbf{p}_1^*, \dots, \mathbf{p}_{2N_{\text{RF}}}^*]^\top$ (to be described later) such that the downlink mmWave RF precoder \mathbf{F}_{RF}^* can be reconstructed from $[\mathbf{p}_1^*, \dots, \mathbf{p}_{2N_{\text{RF}}}^*]^\top$, and the reconstructed \mathbf{F}_{RF}^* maximizes the objective given in (4). Formally, the ideal mapping Ξ is defined as follows

$$\Xi: \mathbb{C}^{2N_{\text{tx}}^{\text{sub-6}} \times K \times T} \rightarrow \mathbb{R}^{2N_{\text{RF}}|\mathcal{C}|}: [\mathbf{h}_1, \dots, \mathbf{h}_T] \mapsto [\mathbf{p}_1^*, \dots, \mathbf{p}_{2N_{\text{RF}}}^*]^\top. \quad (5)$$

In the following, we explain the output design of the ideal mapping Ξ and describe the reconstruction mechanism of \mathbf{F}_{RF}^* from $[\mathbf{p}_1^*, \dots, \mathbf{p}_{2N_{\text{RF}}}^*]^\top$. First, we assume that the output indices $r \in \{1, \dots, N_{\text{RF}}\}$ and $r \in \{N_{\text{RF}} + 1, \dots, 2N_{\text{RF}}\}$ refer to the $+45^\circ$ and -45° polarization, respectively. Second, we assume that the elements of the vector \mathbf{p}_r^* are one-hot encoded, i.e., $(\forall r \in \{1, \dots, 2N_{\text{RF}}\}) \mathbf{p}_r^* \in \{0, 1\}^{|\mathcal{C}|}$, where $|\mathcal{C}|$ indicates the size of a predefined codebook \mathcal{C} . In this way, the indices of the vector $(\forall r \in \{1, \dots, 2N_{\text{RF}}\}) \mathbf{p}_r^*$ are associated with the respective codeword indices from a finite codebook \mathcal{C} . Now, to relate the selected optimal beam indices (in the sense of maximizing the objective in (4)) from a codebook \mathcal{C} for the respective RF chain with the corresponding polarization to the output of the ideal mapping Ξ , we further assume that the each vector $(\forall r \in \{1, \dots, 2N_{\text{RF}}\}) \mathbf{p}_r^*$ contains the value one at the index corresponding to the selected optimal beam index, and zeros elsewhere.

With the output design explained above, the reconstruction of the precoder \mathbf{F}_{RF}^* from $[\mathbf{p}_1^*, \dots, \mathbf{p}_{2N_{\text{RF}}}^*]^\top$ is performed as follows. Once we obtain the output $[\mathbf{p}_1^*, \dots, \mathbf{p}_{2N_{\text{RF}}}^*]^\top$ from Ξ , we construct the precoding matrices $\hat{\mathbf{F}}_{\text{RF}}^*$ and $\tilde{\mathbf{F}}_{\text{RF}}^*$ via

$$\hat{\mathbf{F}}_{\text{RF}}^* = \text{blkdiag}(\hat{\mathbf{f}}_1^*, \dots, \hat{\mathbf{f}}_{N_{\text{RF}}}^*), (\forall r \in \{1, \dots, N_{\text{RF}}\}) \hat{\mathbf{f}}_r^* = \mathbf{c}_{i_r^*} \in \mathcal{C} \quad i_r^* \in \arg \max_{i=1, \dots, |\mathcal{C}|} ([\mathbf{p}_r^*]_i), \quad (6)$$

$$\tilde{\mathbf{F}}_{\text{RF}}^* = \text{blkdiag}(\tilde{\mathbf{f}}_1^*, \dots, \tilde{\mathbf{f}}_{N_{\text{RF}}}^*), (\forall r \in \{1, \dots, N_{\text{RF}}\}) \tilde{\mathbf{f}}_r^* = \mathbf{c}_{i_r^*} \in \mathcal{C} \quad i_r^* \in \arg \max_{i=1, \dots, |\mathcal{C}|} ([\mathbf{p}_{r+N_{\text{RF}}}^*]_i), \quad (7)$$

where $\mathbf{c}_{i_r^*}$ represents the selected optimal codeword from a finite codebook \mathcal{C} by the r^{th} RF chain with corresponding polarization. Further, the precoding matrix \mathbf{F}_{RF}^* that maximizes the objective in (4)

is constructed as $\mathbf{F}_{\text{RF}}^* = [\hat{\mathbf{F}}_{\text{RF}}^* \tilde{\mathbf{F}}_{\text{RF}}^*]^\top$. Although the ideal mapping Ξ solves (4) by assumption, it is challenging to analytically characterize it. Therefore we propose a deep neural network that learns an ideal mapping Ξ from data.

The proposed neural network architecture is given in Fig. 2. With the setting that the RF precoders are taken from a finite codebook, we consider the beam indices as labels and pose the RF precoding problem in (4) as multi-label classification [15]. The labels are constructed as follows. Given a finite codebook \mathcal{C} and a tuple $([\mathbf{h}_1, \dots, \mathbf{h}_T], \mathbf{H}_{T+1})$, where $[\mathbf{h}_1, \dots, \mathbf{h}_T]$ and \mathbf{H}_{T+1} are the T sub-6GHz channel measurements in sequence and the mmWave channel at time step $T + 1$, respectively, we perform an exhaustive search following (4) with \mathbf{H}_{T+1} to obtain \mathbf{F}_{RF}^* . Next, we decompose $\mathbf{F}_{\text{RF}}^* = [\hat{\mathbf{F}}_{\text{RF}}^* \tilde{\mathbf{F}}_{\text{RF}}^*]^\top$ and retrieve $(\forall r \in \{1, \dots, N_{\text{RF}}\}) i_r^*$ by following the rules in (6) and (7). Further, with i_r^* we construct the one-hot encoded ground truth labels $[\mathbf{p}_1^*, \dots, \mathbf{p}_{2N_{\text{RF}}}^*]^\top$.

Given a sequence $[\mathbf{h}_1, \dots, \mathbf{h}_T]$, we extract both the spatially and temporally correlated features from sub-6GHz channel measurements by utilizing convolutional long short-term memory (ConvLSTM) layers. The ConvLSTM layers have a convolutional structure in both the input-to-state and state-to-state transitions. To project the extracted features onto $2N_{\text{RF}}|\mathcal{C}|$ -dimensional vector $[\mathbf{p}_1, \dots, \mathbf{p}_{2N_{\text{RF}}}]^\top$, we customize the task-specific layer based on a fully connected neural network with sigmoid activations so that $(\forall r \in \{1, \dots, 2N_{\text{RF}}\}) \mathbf{p}_r \in [0, 1]^{|\mathcal{C}|}$. With this design, the output of neural network indicates beam priorities. In other words, the index of the first highest value in $(\forall r \in \{1, \dots, 2N_{\text{RF}}\}) \mathbf{p}_r$ is the best suggested beam from the predefined codebook \mathcal{C} . Accordingly, the indices of the second, third and n^{th} highest values, with $n \leq |\mathcal{C}|$, in $(\forall r \in \{1, \dots, 2N_{\text{RF}}\}) \mathbf{p}_r$ are the second, third, and n^{th} best suggestions, respectively. We train a neural network by trying to minimize with the stochastic gradient method the expected value of the binary cross-entropy loss [15] given by

$$\begin{aligned} & \ell([\mathbf{p}_1^*, \dots, \mathbf{p}_{2N_{\text{RF}}}^*]^\top, [\mathbf{p}_1, \dots, \mathbf{p}_{2N_{\text{RF}}}]^\top) = \\ & = -\frac{1}{2N_{\text{RF}}|\mathcal{C}|} \sum_{r=1}^{2N_{\text{RF}}} \sum_{i=1}^{|\mathcal{C}|} ([\mathbf{p}_r^*]_i \log([\mathbf{p}_r]_i) + (1 - [\mathbf{p}_r^*]_i) \log([1 - \mathbf{p}_r]_i)). \end{aligned} \quad (8)$$

In addition to sub-6GHz channel measurements, we also fuse side information to improve the network performance. In more detail, we assume that the UE location information (e.g., Cartesian

coordinates) can be independently acquired by the BS with the use of available positioning technologies. Similar to the sequence of sub-6GHz channel measurements, we construct the sequence with UE location information, i.e., $[\mathbf{v}_1, \dots, \mathbf{v}_T]$, and use a tuple $([\mathbf{h}_1, \dots, \mathbf{h}_T], [\mathbf{v}_1, \dots, \mathbf{v}_T])$ as an input to a neural as show in Fig. 2. To take the advantage of UE location information, we use the fully connected long short-term memory (FC-LSTM) layers.

4. NUMERICAL RESULTS

4.1. Performance Evaluation Metrics

Owing to the fact that the proposed network produces vectors with the elements ranging between 0 and 1, we evaluate the network by measuring the frequency at which the neural network correctly predicts the labels within its *best-n* predictions. The *best-n* prediction accuracy is denoted by $A_{\text{best-n}}$ and it is defined by

$$A_{\text{best-n}} = \frac{1}{S} \sum_{s=1}^S \mathbb{1}_{(\cdot, \cdot)}^n([\mathbf{p}_1^n, \dots, \mathbf{p}_{2N_{\text{RF}}}^n], [\mathbf{p}_1^*, \dots, \mathbf{p}_{2N_{\text{RF}}}^*]), \quad (9)$$

where S is the test dataset size, and $\mathbb{1}_{(\cdot, \cdot)}$ is the indicator function given by

$$\mathbb{1}_{([\mathbf{p}_1^n, \dots, \mathbf{p}_{2N_{\text{RF}}}^n], [\mathbf{p}_1^*, \dots, \mathbf{p}_{2N_{\text{RF}}}^*])} := \begin{cases} 1 & , \text{if } \sum_{r=1}^{2N_{\text{RF}}} \sum_{i=1}^{|C|} [\mathbf{p}_r^n]_i [\mathbf{p}_r^*]_i = 2N_{\text{RF}}, \\ 0 & , \text{otherwise.} \end{cases} \quad (10)$$

The vector \mathbf{p}_r^n represents the predicted labels with the *best-n* criterion, and it contains ones in the indices with the n largest values of \mathbf{p}_r , and zeros elsewhere. In addition to the *best-n* prediction accuracy, we also evaluate the performance of the proposed method in terms of the spectral efficiency with the predicted mmWave beams.

4.2. Simulation

To evaluate the performance of the proposed methods, we generate spatially and time correlated channels with Quasi Deterministic Radio Channel Generator (QuaDRiGa) [16]. The input sequence to the network consists of $T = 5$ spatiotemporal channel measurements, and the proposed method predicts the mmWave beams in $T + 1$ time steps. The finite codebook is adopted from [17]. For network training we use three ConvLSTM layers with the kernel size of 10×10 , and the training and testing datasets consist of 95K and 19K samples, respectively. The learning rate, number of epochs and batch size are 0.001, 10 and 500, respectively. The remaining simulation parameters are given in Table 1. Although the main goal of the proposed method is to skip channel estimation in the mmWave band, as a comparison, we also present the results of the proposed method trained with mmWave channels. The performance of the proposed network trained with sub-6GHz and mmWave channels is denoted

Parameter	Transceiver	
	sub-6GHz	mmWave
Carrier frequency [GHz]	3.6	26
Bandwidth [MHz]	20	800
OFDM subcarriers	$K = 32$	$\bar{K} = 512$
BS antenna size [UPA]	4×4	8×8
UE antenna size	1	2×2 UPA
Polarization	$\pm 45^\circ$	
Signal processing	Fully Digital	HBF with subarray structure ($N_{\text{RF}} = 2$)
Propagation scenario	3GPP_38.901_UMa_NLOS [18]	
UE mobility	30 km/h	

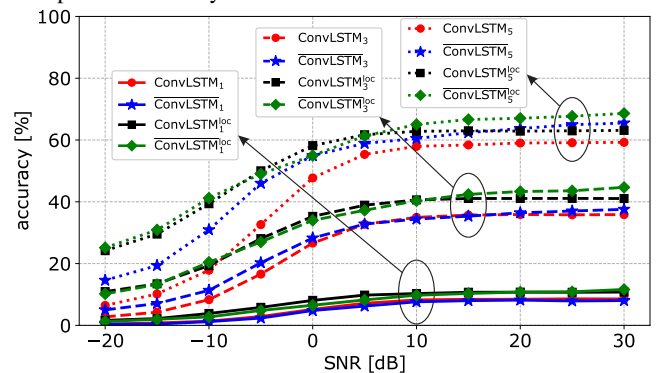
Table 1. Simulation parameters

by ConvLSTM and $\overline{\text{ConvLSTM}}$, respectively. The superscript ^{loc} and the subscripts _{1,3,5} denote the performance with location information and with *best-1,3,5* beam predictions, respectively.

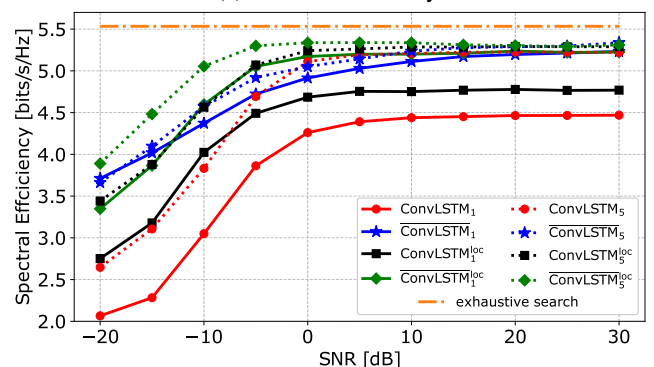
In Fig. 3(a), we compare the prediction accuracy of the proposed method with *best-n* criterion (e.g., $n = 1, 3, 5$) with and without side information. The results in Fig. 3(a) experimentally justify the advantage of fusing side information. In particular, utilization of side information with highly noisy channel measurements improves the performance noticeably.

In Fig.3(b), we provide the spectral efficiency with the beams predicted by the proposed model. The x-axis values represent the SNR of input channel measurements to proposed network and the SNR of mmWave channels, which we utilize to compute the spectral efficiency, is fixed to 30dB. Given $N_{\text{RF}} = 2$ and $|C| = 32$, the exhaustive search method in Fig.3(b) evaluates $|C|^{2N_{\text{RF}}} = 1,048,576$ configurations. In comparison, for $n = 5$, the prediction with *best-n* criterion reduces the search space to 625 configurations.

The results in Fig. 3 demonstrate that the proposed method provides reasonable achievable rates while significantly reducing the signalling overhead. Moreover, exploiting side information can increase the system performance in terms of both prediction accuracy and spectral efficiency.



(a) Prediction accuracy



(b) Spectral efficiency

Fig. 3. Performance of the proposed method.

5. CONCLUSION

In this work, we proposed a deep learning-based hybrid precoding scheme in the mmWave band. The proposed method predicts the mmWave beams by exploiting the spatiotemporal correlation between the sub-6GHz and mmWave bands. Simulations showed that the proposed method can significantly reduce the signalling overhead in mmWave band with hybrid architectures by maintaining good spectral efficiency in the system. Moreover, we showed that side information such as the location of the UE can significantly improve the system performance.

6. REFERENCES

- [1] Omid Semiari, Walid Saad, Mehdi Bennis, and Merouane Debah, "Integrated Millimeter Wave and sub-6GHz Wireless Networks: A Roadmap for Joint Mobile Broadband and Ultra-reliable Low-latency Communications," *IEEE Wireless Communications*, vol. 26, no. 2, pp. 109–115, 2019.
- [2] Robert W Heath, Nuria Gonzalez-Prelcic, Sundeep Rangan, Wonil Roh, and Akbar M Sayeed, "An Overview of Signal Processing Techniques for Millimeter Wave MIMO Systems," *IEEE journal of selected topics in signal processing*, vol. 10, no. 3, pp. 436–453, 2016.
- [3] 3GPP, "Study on New Radio (NR) Access Technology - Physical Layer Aspects - Release 14," *TR 38.802*, 2017.
- [4] Thomas Nitsche, Adriana B Flores, Edward W Knightly, and Joerg Widmer, "Steering with Eyes Closed: Mm-wave Beam Steering without In-band Measurement," in *2015 IEEE Conference on Computer Communications (INFOCOM)*. IEEE, 2015, pp. 2416–2424.
- [5] M Peter, K Sakaguchi, S Jaeckel, S Wu, M Nekovee, J Medbo, K Haneda, SLH Nguyen, R Naderpour, J Vehmas, et al., "Measurement Campaigns and Initial Channel Models for Preferred Suitable Frequency Ranges," *Deliverable D2*, vol. 1, pp. 160, 2016.
- [6] Morteza Hashemi, C Emre Koksall, and Ness B Shroff, "Out-of-band Millimeter Wave Beamforming and Communications to Achieve Low Latency and High Energy Efficiency in 5G Systems," *IEEE transactions on communications*, vol. 66, no. 2, pp. 875–888, 2017.
- [7] Anum Ali, Nuria González-Prelcic, and Robert W Heath, "Millimeter Wave Beam-selection using Out-of-band Spatial Information," *IEEE Transactions on Wireless Communications*, vol. 17, no. 2, pp. 1038–1052, 2017.
- [8] Muhammad Alrabeiah and Ahmed Alkhateeb, "Deep Learning for Mmwave Beam and Blockage Prediction Using Sub-6GHz Channels," *IEEE Transactions on Communications*, 2020.
- [9] Martin Kurras, Sida Dai, Stephan Jaeckel, and Lars Thiele, "Evaluation of the Spatial Consistency Feature in the 3GPP Geometry-Based Stochastic Channel Model," in *2019 IEEE Wireless Communications and Networking Conference (WCNC)*. IEEE, 2019, pp. 1–6.
- [10] Hyun-Ho Lee and Young-Chai Ko, "Low Complexity Codebook-based Beamforming for MIMO-OFDM Systems in Millimeter-wave WPAN," *IEEE Transactions on Wireless Communications*, vol. 10, no. 11, pp. 3607–3612, 2011.
- [11] Andrea Goldsmith, Syed Ali Jafar, Nihar Jindal, and Sriram Vishwanath, "Capacity Limits of MIMO Channels," *IEEE Journal on selected areas in Communications*, vol. 21, no. 5, pp. 684–702, 2003.
- [12] Omar El Ayach, Sridhar Rajagopal, Shadi Abu-Surra, Zhouyue Pi, and Robert W Heath, "Spatially Sparse Precoding in Millimeter Wave MIMO Systems," *IEEE transactions on wireless communications*, vol. 13, no. 3, pp. 1499–1513, 2014.
- [13] Ahmed Alkhateeb and Robert W Heath, "Frequency Selective Hybrid Precoding for Limited Feedback Millimeter Wave Systems," *IEEE Transactions on Communications*, vol. 64, no. 5, pp. 1801–1818, 2016.
- [14] Sungwoo Park, Ahmed Alkhateeb, and Robert W Heath, "Dynamic Subarrays for Hybrid Precoding in Wideband mmWave MIMO Systems," *IEEE Transactions on Wireless Communications*, vol. 16, no. 5, pp. 2907–2920, 2017.
- [15] Grigorios Tsoumakas and Ioannis Katakis, "Multi-label Classification: An Overview," *International Journal of Data Warehousing and Mining (IJDWM)*, vol. 3, no. 3, pp. 1–13, 2007.
- [16] S Jaeckel, L Raschkowski, K Börner, L Thiele, F Burkhardt, and E Eberlein, "QuaDRiGa-Quasi Deterministic Radio Channel Generator, User Manual and Documentation," *Fraunhofer Heinrich Hertz Institute, Tech. Rep. v1*, pp. 4–1, 2016.
- [17] Yi Xie, Shi Jin, Jue Wang, Yongxu Zhu, Xiqi Gao, and Yongming Huang, "A Limited Feedback Scheme for 3D Multiuser MIMO based on Kronecker Product Codebook," in *2013 IEEE 24th Annual International Symposium on Personal, Indoor, and Mobile Radio Communications (PIMRC)*. IEEE, 2013, pp. 1130–1135.
- [18] 3GPP TR 38.901 v 14.1.0, "Study on Channel Model for Frequencies from 0.5 to 100 GHz," *Tech. Rep.*, 2017.